Manganese-Based Layered Coordination Polymer: Synthesis, Structural Characterization, Magnetic Property, and Electrochemical Performance in Lithium-Ion Batteries

Qi Liu,*[†,‡] Lili Yu,[‡] Ying Wang,[†] Yunzhou Ji,[‡] Josip Horvat,[§] Mei-Ling Cheng,[‡] Xiaoyan Jia,[‡] and Guoxiu Wang*[†]

[†]Centre for Clean Energy Technology, School of Chemistry and Forensic Science, University of Technology Sydney, Broadway, Sydney, New South Wales 2007, Australia

[‡]School of Petrochemical Engineering, Changzhou University, Changzhou 213164, P. R. China

[§]Institute for Superconducting and Electronic Materials, University of Wollongong, New South Wales 2522, Australia

Ⓢ Supporting Information

ABSTRACT: Manganese-based layered coordination polymer ([Mn-(tfbdc)(4,4'-bpy)(H$_2$O)$_2$], Mn−LCP) with microporous structure was synthesized by reaction of 2,3,5,6-tetrafluoroterephthalatic acid(H$_2$tfbdc) and 4,4'-bipyridine(4,4'-bpy) with manganese(II) acetate tetrahydrate in water solution. Mn−LCP was characterized by elemental analysis, IR spectra, thermogravimetric analysis, X-ray single-crystal structure analysis, and powder X-ray diffraction. Magnetic susceptibility data from 300 to 1.8K show that there is a weak antiferromagnetic exchange between Mn(II) ions in Mn−LCP. As anode material, the Mn−LCP electrode exhibits an irreversible high capacity in the first discharge process and a reversible lithium storage capacity of up to about 390 mA h/g from the fourth cycle. It might provide a new method for finding new electrode materials in lithium-ion batteries
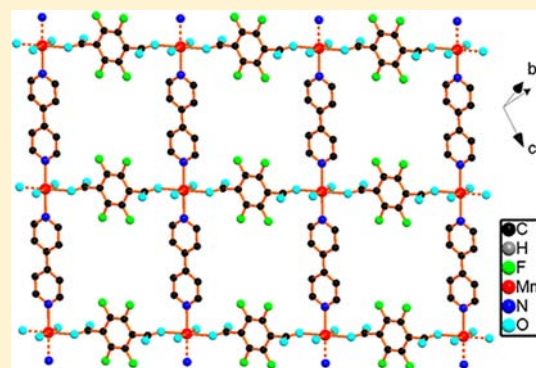
1. INTRODUCTION

In recent years, metal−organic frameworks (MOFs) or coordination polymers with porous structures have received considerable attention for their unique physical and chemical properties and many potential applications.[1,2] Self-assembly of metal-ion and/or metal clusters with varieties of organic linkers has not only led to a unique type of porous materials for gas storage,[3,4] selective separation,[5] catalysis,[6] and drug delivery[7] but also produced a series of functional materials with special magnetic, nonlinear optical, and luminescent properties.[8−10] In particular, multibenzenecarboxylate ligands have been shown to be good building blocks in the design of metal−organic materials with desired topologies owing to their rich coordination modes. One of the most frequently used linker ligands is the dianion of terephthalic acid (H$_2$bdc), from which two of the most prominent members of this class of compounds, MOF-5[11] and MIL-53,[12] are constructed. The perfluorinated terephthalic acid, that is, 2,3,5,6-tetrafluoroter-ephthalic acid (H$_2$tfbdc), is also a versatile building block for construction of metal−organic complexes through complete or partial deprotonation of its carboxyl groups, and some interesting structures have been successfully obtained.[13−17] Recently, we obtained several complexes with 2,3,5,6-tetrafluoroterephthalate via self-assembly of H$_2$tfbdc with transition metal ions under mild solution synthetic conditions.[18,19] Considering the special bioactive function of

manganese carboxylate complexes along with their interesting magnetic properties[20] and the interesting hydrogen storage properties of porous MOFs containing exposed fluorine atoms,[21] we continue to investigate materials with tetrafluor-oterephthalate (tfbdc) and extend this work to the system of Mn(II), H$_2$tfbdc, and 4,4'-bipyridine (4,4'-bpy). The 4,4'-bpy ligand has been extensively used in synthesizing one-dimensional to three-dimensional coordination polymers with catalytic, magnetic, unusual nonlinear optical, and conductive properties.[2,6b,22,23]

On the other hand, in order to improve the energy density and thermal stability of lithium-ion batteries, many new inorganic-based and organic-based electrode materials have been synthesized.[24,25] There have also been a few reports on the electrochemical performance of three-dimensional (3D) microporous metal−organic frameworks in lithium-ion bat-teries.[26−29] For example, G. Férey et al.[26] reported that MIL-53(Fe) or Fe^{III}(OH)$_{0.8}$F$_{0.2}$[O$_2$C−C$_6$H$_4$−CO$_2$] shows a rever-sible electrochemical Li insertion with a very good cycling life as a cathode material in lithium cells. It is a pity that its capacity (70 mAh/g) is far lower than that of the commonly used LiCoO$_2$. On the basis of the facts that LiCoO$_2$ cathode material and carbon anode material have all layered structures, MOFs or

coordination polymers with two-dimensional (2D) layered structures can also be candidates as electrode materials for lithium-ion cells, considering that from the viewpoint of material structure the metal cations with variable valence can be active sites of redox reactions.[26,30] However, to the best of our knowledge, to date there have been few reports on the electrochemical performance of 2D layered coordination polymers in lithium batteries.[31] Herein, we report the synthesis, crystal structure, and magnetic property of a 2D manganese-based coordination polymer ($[Mn(tfbdc)(4,4'-bpy)(H_2O)_2]$, Mn−LCP) and the electrochemical performance of it as an anode material for lithium-ion batteries.

2. EXPERIMENTAL SECTION

2.1. Materials. 2,3,5,6-Tetrafluoroterephthalic acid (H_2tfbdc), manganese(II) acetate tetrahydrate, 4,4′-bipyridine (4,4′-bpy), and solvents were of reagent grade without further purification before use.

2.2. Synthesis of [Mn(tfbdc)(4,4′-bpy)(H₂O)₂]. A 5 mL amount of a deionized water solution of $Mn(OAc)_2 \cdot 4H_2O$ (0.0245g, 0.10 mmol) was slowly added to 5 mL of a deionized water solution that contained H_2tfbdc (0.0238 g, 0.10 mmol) and 4,4′-bpy (0.0078 g, 0.05 mmol) to afford a colorless solution. Upon slow evaporation of the solvent at room temperature for several days, colorless block crystals of $[Mn(tfbdc)(4,4'-bpy)(H_2O)_2]$(Mn-LCP) were obtained. Anal. Calcd for $C_{18}H_{12}F_4MnN_2O_6$: C, 44.74; H, 2.50; N, 5.80. Found: C, 44.70; H, 2.55; N, 5.76. IR data (cm⁻¹, KBr pellet): 3460 (s), 3205 (w), 1605 (vs), 1535(m), 1492(w), 1469 (s), 1414 (w), 1386(vs), 1254 (w), 1218(m), 1131(w), 1068 (m), 1044(m), 1006(w), 982 (s), 806 (s), 733 (s), 686 (s), 648(w), 629 (s), 474 (s).

2.2. Physical Measurements. Elemental analysis (C, H, and N) was performed on a Perkin-Elmer 2400 Series II element analyzer. FTIR spectra were recorded on a Nicolet 460 spectrophotometer in the form of KBr pellets. Thermogravimetric analysis (TGA) experiments were carried out on a Dupont thermal analyzer from room temperature to 800 °C under N_2 atmosphere at a heating rate of 10 °C/min. The X-ray photoelectron spectrum of Mn−LCP was taken on an ESCALAB MK II X-ray photoelectron spectrometer using a nonmonochromatized Mg Kα X-ray as the excitation source and choosing C1s (284.6 eV) as the reference line. Magnetic measurements of the samples were performed on a SQUID magnetometer.

2.3. Electrochemical Measurement. For electrochemical testing, Mn−LCP was dried for about 6 h at 50 °C in the vacuum oven prior to being opened in an argon atmosphere. Electrodes were prepared mixing crystalline Mn−LCP (80 wt %) with 10 wt % carbon black (Super P, MMM, Belgium) and 10 wt % polyvinylidene fluoride binder in N-methyl-2-pyrrolidinone solvent to form a homogeneous slurry. Then, the slurry was spread onto a copper foil. Coated electrodes were dried in a vacuum oven at 80 °C for 12 h and then pressed. Electrochemical measurements were carried out using coin-type cells. CR 2032 coin-type cells were assembled in an argon-filled glovebox (Mbraun, Unilab, Germany) by stacking a porous polypropylene separator containing liquid electrolyte between the composite electrodes and a lithium-foil counter electrode. Electrolyte used was 1 M $LiPF_6$ in a 50:50 (v/v) mixture of ethylene carbonate and dimethyl carbonate obtained from MERCK KgaA, Germany. Cells were galvanostatically charged and discharged in the range of 0.01−2.5 V at a constant current density of 50 mAg⁻¹.

2.4. X-ray Crystallography. Single-crystal X-ray diffraction measurement of Mn−LCP was carried out with a Bruker Smart Apex CCD diffractometer at 291(2) K. Intensities of reflections were measured using graphite-monochromatized Mo Kα radiation (λ = 0.071073 nm) with the ψ−ω scans mode in the range of 2.53° ≤ θ ≤ 25.99°. The structure was solved by direct methods using the SHELXTL-97[32]computer program and refined by full-matrix least-squares methods on F^2 with the SHELXTL-97 program package. Anisotropic thermal factors were assigned to all non-hydrogen atoms. Hydrogen atoms were included in calculated positions and refined with isotropic thermal parameters riding on the parent atoms.

Crystallographic data for structural analyses are summarized in Table 1.

Table 1. Crystal Structure Parameters of Mn−LCP

formula	$C_{18}H_{12}F_4MnN_2O_6$	calcd density/ (g·cm⁻³)	1.740
fw	483.24	Mu(Mo Kα)/ mm⁻¹	0.797
cryst size/ mm	0.24 × 0.26 × 0.30	index ranges (h, k, l)	−8/8, −9/9, −10/10
cryst syst	triclinic	F(000)	243
space group	P$\bar{1}$	no. of reflns collected	4138
a/Å	7.136(1)	no. of independent reflns	1807 (R_{int} = 0.0492)
b/Å	8.079(3)	no. of obsd reflns	1278
c/Å	8.522(2)	data/ restraints/ params	1807/0/ 142
α/deg	90.55(2)	goodness of fit on F^2	0.956
β/deg	109.29(1)	R_1, wR_2 [$I > 2\sigma(I)$]	0.0609, 0.1183
γ/deg	95.35(2)	R_1, wR_2 (all data)	0.0807, 0.1243
V/Å³	461.3(2)	largest diff. peak and hole/e·Å⁻³	0.511 and −0.277
Z	1		

3. RESULTS AND DISCUSSION

3.1. Crystal Structure Description of [Mn(tfbdc)(4,4′-bpy)(H₂O)₂]. As shown in Figure 1, the Mn(II) ion has an octahedral geometry coordinated by two O atoms from two tfbdc dianions, two O atoms from two waters, and two N atoms from two 4,4′-bpy molecules. N(1C), O(2), N(1), and O(2C) atoms are in the equatorial position [Mn(1)−N(1C) = 2.309(3) Å, Mn(1)−O(2C) = 2.185(3) Å]; O(3C) and O(3) atoms are in the axial position [Mn(1)−O(3) =2.251(3)
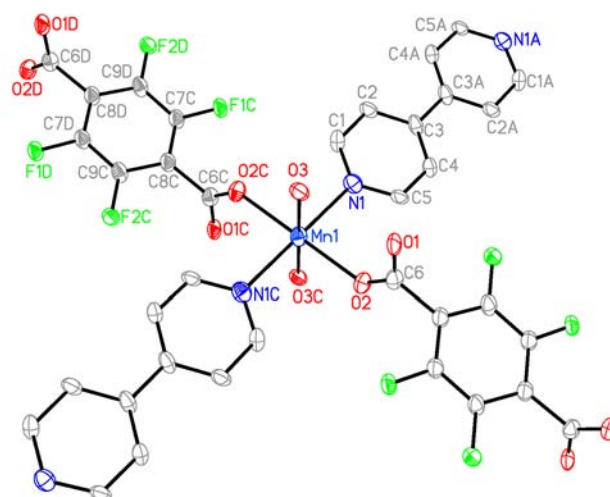
Symmetry code: A: 1-x,1-y,-1-z; C: 2-x,2-y,-z; D: x,-1+y,z

Figure 1. Structure unit of $[Mn(tfbdc)(4,4'-bpy)(H_2O)_2]$ (hydrogen atoms omitted for clarity).

Å]. The average bond length of Mn−N (0.2309 nm) is longer than that of Mn−O (2.218 Å). The bond angles of O(3)−Mn(1)−O(3C), N(1)−Mn1−N(1C), and O(2)−Mn(1)−O(2C) are all 180.00°, further indicating the Mn(II) ion has octahedral geometry. Each 4,4′-bpy and tfbdc dianion bridges two Mn(II) ions to form a 2D microporous layer with (4,4) topological network, as shown in Figure 2. The shortest
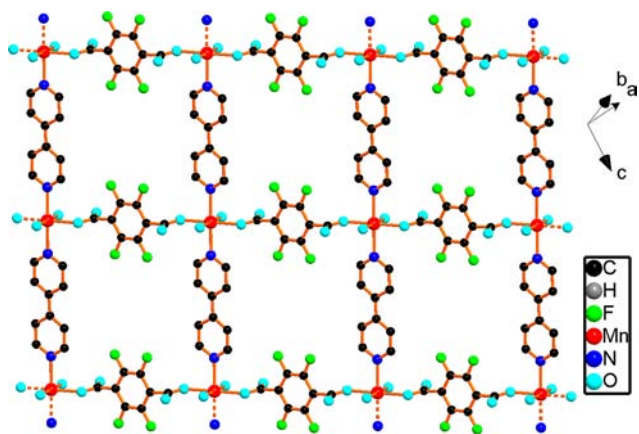

Figure 2. Two-dimensional layer structure of Mn−LCP.

distance Mn(II)−Mn(II) in the same layer is 11.686 Å. The 2D structure of Mn−LCP is quite similar to that of [M(NDA)-(4,4′-bpy)(H$_2$O)$_2$]·nH$_2$O and [Mn(o-phth) 4,4′-bpy)(H$_2$O)$_2$]$_n$ reported previously.[33] Hydrogen-bonding interactions between the layers [O3−H3A---F2 = 3.252(4) Å, O3−H3C---O1= 2.753(4) Å, and C1−H1---O2 = 3.192(4) Å] leads to formation of a 3D network with tunnels as shown in Figure 3.
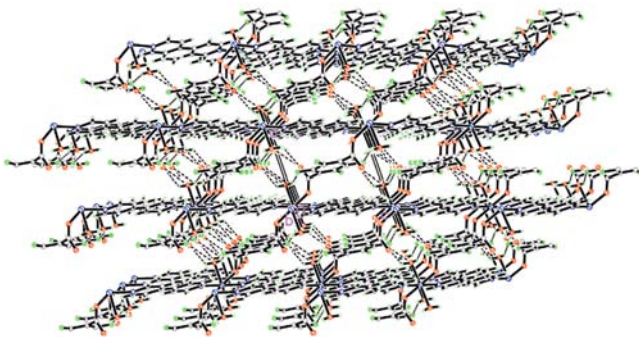

Figure 3. Packing diagram of Mn−LCP viewed along the b axis; dashed lines indicate there are hydrogen bonds between the layers.

Figure 4 shows the powder X-ray diffraction (XRD) pattern of as-synthesized Mn−LCP and vacuum-dried Mn−LCP at 50 °C for 6 h. X-ray powder diffraction peak positions for vacuum-dried Mn−LCP are the same as those of Mn−LCP, showing it does not lose coordination water molecules and retains the same structure of Mn−LCP.

3.2. Thermal Stability. TGA for Mn−LCP shows that weight loss begins at 182 °C, indicating the framework of Mn−LCP is stable at 182 °C. Weight loss from 182 to 249 °C corresponds to two coordinated water molecules removed per formula unit (calcd 7.46%, found 7.01%), and another weight loss between 249 and 348.6 °C is ascribed to 4,4′-bpy molecule removal (calcd 32.32%, found 35.97%) (see Supporting Information Figure S1).
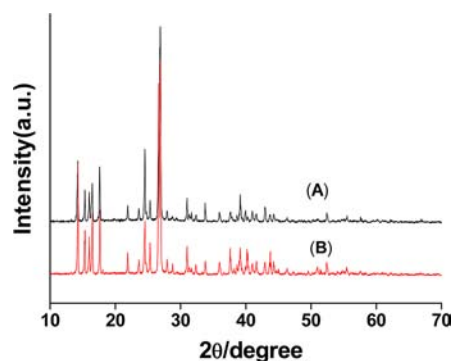

Figure 4. Powder X-ray diffraction pattern of the as-synthesized Mn−LCP (A) and Mn−LCP after being vacuum dried at 50 °C for 6 h (B).

3.3. Infrared Spectrum. The IR spectrum of Mn−LCP reflects the binding patterns of 4,4′-bpy, H$_2$O, and 2,3,5,6-tetrafluoroterephthalate (tfbdc). The strong absorption band in the 3600−3200 cm^{-1} region corresponds to ν(OH) of the coordination water molecules. All carboxylic groups are deprotonated, as indicated by no absorption around 1730 cm^{-1} for a protonated carboxylic group. Strong peaks at 1605 and 1386 cm^{-1} are the ν_{as}(OCO) and ν_s(OCO) stretching modes of coordinated tfbdc, respectively, while strong absorption at ca. 733 cm^{-1} is the δ(OCO) bent vibration of tfbdc.[19] The difference of 219 cm^{-1} between ν_{as}(OCO) and ν_s(OCO) indicates that the tfbdc ligands adopt an amphimonodentate coordination mode[34−36] as proved by X-ray crystal structure analysis of Mn−LCP. The absorption bands at ca. 3205 and 806 cm^{-1} are ν(C−H) stretching and bent vibrations of 4,4′-bipy, respectively.[37] The IR spectrum of vacuum-dried Mn−LCP at 50 °C is the same as that of the as-synthesized Mn−LCP, which indicates that such a vacuum-drying step cannot sufficiently remove the coordinated water molecules of the compound due to the stable nature of the compound below 182 °C (Supporting Information Figure S2).

3.4. Magnetic Property. The temperature dependence of the magnetic susceptibility of Mn−LCP was measured from 2 to 300 K with a Quantum Design SQUID magnetometer in an applied magnetic field of 2000 Oe; data are shown in Figure 5 as plots of $\chi_M T$ and χ_M^{-1} versus T. The $\chi_M T$ product is 4.386 emu K mol^{-1} at 300 K, which is close to the value expected for the spin-only value of the Mn(II) ion (4.376 emu K mol^{-1} with
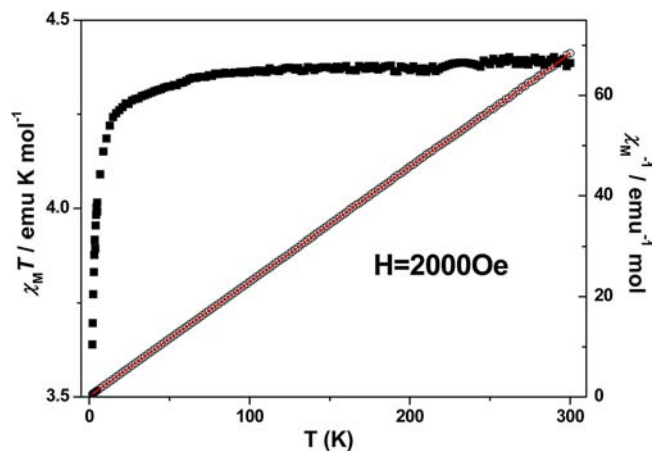

Figure 5. Temperature dependence of $\chi_M T$ (■) and χ_M^{-1} (○) for Mn−LCP.

$g = 2.0$). The $\chi_m T$ value decreases gradually on cooling, and a value of 3.639 emu K mol^{-1} is reached at 2 K. Data can be fitted nicely to the Curie–Weiss law, yielding $C = 4.4$ emu K mol^{-1} and $\Theta = -0.74$ K. The results show the occurrence of very weak antiferromagnetic interactions between the Mn(II) centers in Mn–LCP.

3.5. Electrochemical Performance for Lithium Storage. The electrochemical performance of Mn–LCP for lithium storage in lithium-ion cells was investigated by cyclic voltammetry (CV) and a galvanostatic charge/discharge cycling test. Figure 6a shows the CV curves of the Mn–LCP electrode
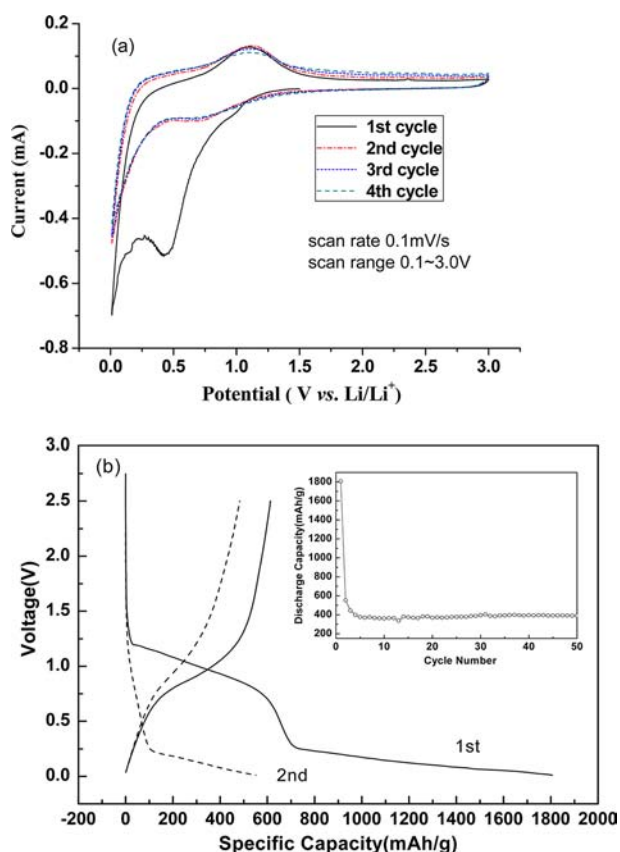

Figure 6. (a) CV curves of the Mn−LCP electrode. (b) Charge/discharge profiles of the Mn−LCP electrode in a lithium-ion cell. (Inset) Discharge capacity vs cycle number from the second cycle.

in the voltage range of 0.1−3.0 V. The cathodic peak at around 0.45 V should correspond to $[Li_2(tfbdc)(4,4'-bpy)]$ formation during the first discharge (eq 1 below).

The peak at around 0.45 V disappears after the first discharge, leaving an initial irreversible capacity, as shown in Figure 6b. The cathodic peaks at around 0.1 and 0.7 V during discharging and the broad anodic peak at 0.75−1.4 V during the charging process, which may be assigned to the reduction and oxidation peaks of the Mn(II)/Mn pair, will be mentioned later. Figure 6b shows the charge/discharge profiles of the Mn−LCP electrode. The cycling performance (reversible lithium storage vs cycle number) is shown as the inset in Figure 6b. The first discharge capacity of the Mn−LCP electrode is 1807 mAh/g, but the second discharge capacity is only 552 mA h/g. Compared with the capacity of the first and second cycles, capacity loss is as high as 69.5%. However, from the fourth cycle, the Mn−LCP electrode demonstrates a stable capacity for reversible lithium storage. After 50 cycles, the electrode

maintains a capacity of about 390 mAh/g, indicating good cycling stability of the Mn−LCP electrode.

To learn about the electrochemical reactions in the Mn−LCP electrode, we examined FTIR spectra of the Mn−LCP electrodes and electrolyte; the results are shown in Figure 7.
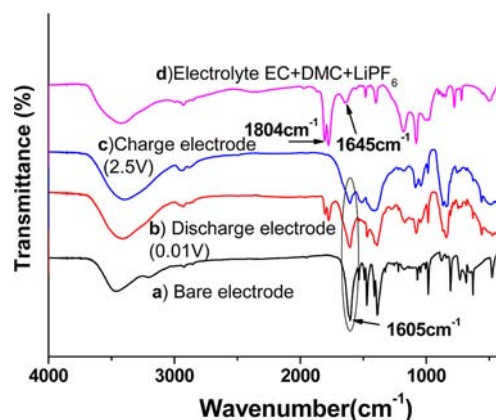

Figure 7. FTIR spectra of the Mn−LCP (a) bare electrode, (b) discharge at 0.01 V, (c) charge at 2.5 V, and (d) electrolyte containing ethylene carbonate (EC), dimethyl carbonate (DMC), and LiPF$_6$.

The fact that the characteristic peak of the carboxylate group from the tfbdc anion at 1605 cm^{-1} appears in FTIR spectra of the bare electrode, the discharged and charged electrodes, shows the tfbdc anions are reversibly involved in the cycling. For confirming changes in the oxidation state of manganese under discharge and charge states, magnetic measurements of used and unused electrodes were carried out. As shown in Figure 8, after the first discharge to 0.01 V, the magnetic
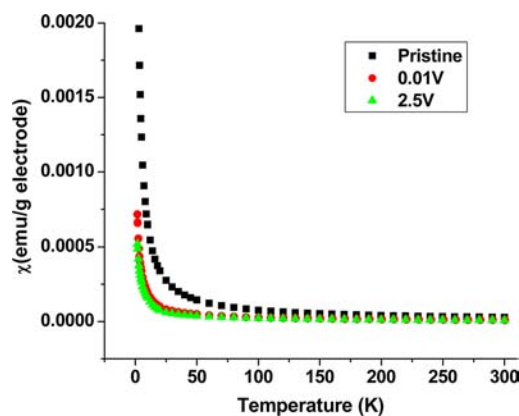

Figure 8. Temperature dependence of magnetic susceptibility (χ) for selected samples: pristine electrode prepared with Mn−LCP (■), 0.01 V (○), and 2.5 V (△).

susceptibility value ($\chi^{100K} = 2.681 \times 10^{-5}$ emu g^{-1}) of electrode materials is lower than that of the pristine electrode materials consisting of Mn−LCP, carbon black, and binder additives ($\chi^{100K} = 7.640 \times 10^{-5}$ emu g^{-1}), which agrees with loss of Mn^{2+} and occurrence of Mn^0; a similar change has been observed in the MnCO$_3$ electrode.[38] After battery recharge to 2.5 V, the magnetic susceptibility value of electrode materials at 100 K is different with that of the pristine electrode materials, showing Mn−LCP is not recovered and Mn(II) ions have different chemical environments in the pristine and charge electrode materials. To further ascertain the valence state of manganese

after the first discharge, XPS spectra of the Mn−LCP samples taken before and after the first discharge processes were recorded (Supporting Information, Figure S3). As shown in Figure S3, Supporting Information, the XPS spectrum of pristine Mn−LCP (Supporting Information, Figure S3a) is different from that of the Mn−LCP sample performed after the first discharge (Figure S3b, Supporting Information), indicating the varied chemical state of the manganese element. In Figure S3a, Supporting Information, the two peaks appearing at 641.8 and 653.9 eV can be assigned to Mn2p$_{3/2}$ and Mn2p$_{1/2}$ of Mn(II) ions, respectively,[39] while in Figure S3b, Supporting Information, the two peaks appearing at 638.5 and 650 eV can be assigned to Mn2p$_{3/2}$ and Mn2p$_{1/2}$ of metallic manganese, respectively. The binding energy difference of 11.5 eV between Mn2p$_{3/2}$ and Mn2p$_{1/2}$ is in accord with the value reported in the literature.[39] These facts all confirm formation of metallic manganese after the first discharge. In addition, because the change of the coordination environment of the metal ion can result in a slight change of its binding energy,[39] the two peaks appearing at 641.1 and 653.6 eV can be also assigned to Mn2p$_{3/2}$ and Mn2p$_{1/2}$ of Mn(II) ions, respectively, which indicate Mn(II) ions still exist in the sample after the first discharge. These Mn(II) ions may be a result from the oxidation product of metallic manganese during the sample transfer process/the unreduced Mn(II) ions during the first discharge process.

On the basis of the experimental results above, we speculate that the possible conversion reaction in the Mn−LCP electrode could be expressed as

$$[Mn(tfbdc)(4, 4'\text{-bpy})(H_2O)_2] + 2Li^+ + 2e$$
$$\rightarrow Mn + [Li_2(tfbdc)(4, 4'\text{-bpy})] \qquad (1)$$
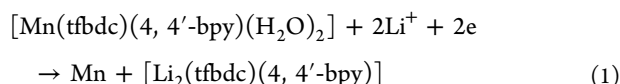
In the first discharge process, $[Mn(tfbdc)(4,4'\text{-bpy})(H_2O)_2]$ reacts with Li via conversion reaction, leading to formation of Mn, and the tfbdc compound of Li ions (using $[Li_2(tfbdc)(4,4'\text{-bpy})]$ stand for it), as shown in eq 1. A similar conversion reaction has been observed in a 3D $Zn_3(HCOO)_6$ MOF electrode.[40] Large irreversible capacity loss (ICL) at the first charge cycle might be attributed to the coordination water of Mn−LCP and electrolyte decomposition, as observed in $Zn(HCOO)_2\cdot2H_2O$ electrode,[40] while ICL is mainly due to electrolyte decomposition after the first cycle. Similar irreversible cycle phenomena have been also observed in SnO_2 nanowires and graphene electrodes for lithium batteries.[41] For reducing ICL, prelithiation of the Mn−LCP-based electrode[42] and tailoring of the inherent transport properties of coordination polymers may be good routes. Besides, except for the contribution from the Mn(II)/Mn pair, the capacity of the Mn−LCP electrode material might be also related to the capacitive contribution and the pseudocapacitive contribution as $MnCO_3$ electrode material.[38] Further study will be needed to learn about more detailed electrochemical behavior of the Mn−LCP electrode.

4. CONCLUSION

We successfully synthesized the 2D Mn-based coordination polymer $[Mn(tfbdc)(4,4'\text{-bpy})(H_2O)_2]$, Mn−LCP. Mn−LCP exhibited a very weak antiferromagnetic coupling between Mn(II) ions. When Mn−LCP was applied as an anode material in lithium-ion cells, it delivered an irreversible high capacity in the first discharge process and a reversible lithium storage capacity up to about 390 mA h/g from the fourth cycle.

Though its capacity is not considerable high due to the conversion reaction of Mn−LCP, the lower capacity problem of metal coordination polymer materials may be solved by applying a compound containing variable valence metal ions (Fe^{III} ion et al), as 3D compound $Fe^{III}(OH)_{0.8}F_{0.2}[O_2C−C_6H_4−CO_2]$,[26] which is stable during lithium-ion insertion and extraction. Thus, it is possible to obtain stable 2D metal coordination polymers with good electrochemical performance via self-assembly of variable-valence metal ions and organic ligands with low molecular weight. It might be a new route to look for electrode materials of lithium cells from 2D metal coordination polymers. Further investigation based on 2D coordination polymers is still in progress.

■ ASSOCIATED CONTENT

Ⓢ Supporting Information

TGA curve, IR spectra, XPS spectra, CIF file. This material is available free of charge via the Internet at http://pubs.acs.org.

■ AUTHOR INFORMATION

Corresponding Author
*E-mail: liuqi62@163.com; Guoxiu.Wang@uts.edu.au.

Notes
The authors declare no competing financial interest.

■ REFERENCES

(1) Férey, G. *Chem. Soc. Rev.* **2008**, *37*, 191.
(2) Kitagawa, S.; Kitaura, R.; Noro, S. *Angew. Chem., Int. Ed.* **2004**, *43*, 2334.
(3) (a) Rosi, N. L.; Eckert, J.; Eddaoudi, M.; Vodak, D. T.; Kim, J.; O'Keeffe, M.; Yaghi, O. M. *Science* **2003**, *300*, 1127. (b) Choi, H. J.; Dincă, M.; Long, J. R. *J. Am. Chem. Soc.* **2008**, *130*, 7848. (c) Dincă, M.; Long, J. R. *Angew. Chem., Int. Ed.* **2008**, *47*, 6766. (d) Jeon, Y. M.; Armatas, G. S.; Heo, J.; Kanatzidis, M. G.; Mirkin, C. A. *Adv. Mater.* **2008**, *20*, 2105.
(4) (a) Li, H.; Eddaoudi, M.; Groy, T. L.; Yaghi, O. M. *J. Am. Chem. Soc.* **1998**, *120*, 8571. (b) Millward, A. R.; Yaghi, O. M. *J. Am. Chem. Soc.* **2005**, *127*, 17998. (c) Deng, H.; Doonan, C. J.; Furukawa, H.; Ferreira, R. B.; Towne, J.; Knobler, C. B.; Wang, B.; Yaghi, O. M. *Science* **2010**, *327*, 846. (d) Eddaoudi, M.; Kim, J.; Rosi, N.; Vodak, D.; Wachter, J.; O'Keeffe, M.; Yaghi, O. M. *Science* **2002**, *295*, 469.
(5) (a) Wang, B.; Côté, A. P.; Furukawa, H.; O'Keeffe, M.; Yaghi, O. M. *Nature* **2008**, *453*, 207. (b) Cychosz, K. A.; Wong-Foy, A. G.; Matzger, A. J. *J. Am. Chem. Soc.* **2008**, *130*, 6938.
(6) (a) Ohara, K.; Kawano, M.; Inokuma, Y.; Fujita, M. *J. Am. Chem. Soc.* **2010**, *132*, 30. (b) Fujita, M.; Kwon, Y. J.; Washizu, S.; Ogura, K. *J. Am. Chem. Soc.* **1994**, *116*, 1151. (c) Ma, L. Q.; Abney, C.; Lin, W. B. *Chem. Soc. Rev.* **2009**, *38*, 1248. (d) Zou, R. Q.; Sakurai, H.; Han, S.; Zhong, R. Q.; Xu, Q. *J. Am. Chem. Soc.* **2007**, *129*, 8402. (e) Hasegawa, S.; Horike, S.; Matsuda, R.; Furukawa, S.; Mochizuki, K.; Kinoshita, Y.; Kitagawa, S. *J. Am. Chem. Soc.* **2007**, *129*, 2607.
(7) Horcajada, P.; Serre, C.; Maurin, G.; Ramsahye, N. A.; Balas, F.; Vallet-Regí, M.; Sebban, M.; Taulelle, F.; Férey, G. *J. Am. Chem. Soc.* **2008**, *130*, 6774.
(8) (a) Milon, J.; Daniel, M.; Kaiba, A.; Guionneau, P.; Brandés, S.; Sutter, J. *J. Am. Chem. Soc.* **2007**, *129*, 13872. (b) Cui, H.; Wang, Z.;

Takahashi, K.; Okano, Y.; Kobayashi, H.; Kobayashi, A. *J. Am. Chem. Soc.* **2006**, *128*, 15074.

(9) Guo, Z.; Cao, R.; Wang, X.; Li, H.; Yuan, W.; Wang, G.; Wu, H.; Li, J. *J. Am. Chem. Soc.* **2009**, *131*, 6894.

(10) (a) Bauer, C. A.; Timofeeva, T. V.; Settersten, T. B.; Patterson, B. D.; Liu, V. H.; Simmons, B. A.; Allendorf, M. D. *J. Am. Chem. Soc.* **2007**, *129*, 7136. (b) Zhao, B.; Chen, X. Y.; Cheng, P.; Liao, D. Z.; Yan, S. P.; Jiang, Z. H. *J. Am. Chem. Soc.* **2004**, *126*, 15394.

(11) Li, H.; Eddaoudi, M.; O'Keeffe, M.; Yaghi, O. M. *Nature* **1999**, *402*, 276.

(12) Loiseau, T.; Serre, C.; Huguenard, C.; Fink, G.; Taulelle, F.; Henry, M.; Bataille, T.; Férey, G. *Chem.—Eur. J.* **2004**, *10*, 1373.

(13) Ryo, K.; Fumiyasu, I.; Ryotaro, M.; Kitagawa, S.; Kubota, Y.; Takata, M.; Kobayashi, T. C. *Inorg. Chem* **2004**, *43*, 6522.

(14) Mitsuhiro, I.; Satoru, O. *Inorg. Chim. Acta* **2004**, *357*, 1039.

(15) Rau, S.; Böttcher, L.; Schebesta, S.; Stollenz, M.; Görls, H.; Walther, D. *Eur. J. Inorg. Chem.* **2002**, 2800.

(16) Chen, B. L.; Yang, Y.; Fatima, Z.; Qian, G. D.; Luo, Y. S.; Zhang, J. H.; Lobkovsky, E. B. *Inorg. Chem* **2006**, *45*, 8882.

(17) Hyungphil, C.; Danil, N. D.; Hyunuk, K.; Kim, K. *Chem.—Eur. J.* **2005**, *11*, 3521.

(18) Zhu, E. J.; Liu, Q.; Chen, Q.; He, M. Y.; Chen, S. C.; Huang, H.; Yang, Q. *Chin. J. Inorg. Chem.* **2008**, *24*, 1428.

(19) (a) Zhu, E. J.; Liu, Q.; Chen, Q.; He, M. Y.; Chen, S. C.; Huang, H. *J. Coord. Chem.* **2009**, *62*, 2449. (b) Cheng, M. L.; Zhu, E. J.; Liu, Q.; Chen, S. C.; Chen, Q.; He, M. Y. *Inorg. Chem. Commun.* **2011**, *14*, 300.

(20) Gopalan, R.; Muralee, M.; Carolina, S. E.; Monica, S.; Wolfgang, W.; Madeleine, H.; Chris, M.; Jim, R.; Simon, J. T.; George, C.; Euan, K. B. *J. Am. Chem. Soc.* **2004**, *126*, 15445.

(21) Hulvey, Z.; Falcao, E. H. L.; Eckert, J.; Cheetham, A. K. *J. Mater. Chem.* **2009**, *19*, 4307.

(22) Feller, R. K.; Cheetham, A. K. *Dalton Trans.* **2008**, 2034.

(23) Phuengphai, P.; Youngme, S.; Gamez, P.; Reedijk, J. *Dalton Trans.* **2010**, *39*, 7936.

(24) (a) Armand, M.; Tarascon, J. M. *Nature* **2008**, *451*, 652. (b) Kang, K. S.; Meng, Y. S.; Breger, J.; Grey, C. P.; Ceder, G. *Science* **2006**, *311*, 977. (c) Whittingham, M. S. *Chem. Rev.* **2004**, *104*, 4271.

(25) (a) Walker, W.; Grugeon, S.; Mentre, O.; Laruelle, S.; Tarascon, J. M.; Wudl, F. *J. Am. Chem. Soc.* **2010**, *132*, 6517. (b) Han, X. Y.; Chang, C. X.; Yuan, L. J.; Sun, T. L.; Sun, J. T. *Adv. Mater.* **2007**, *19*, 1616.

(26) Férey, G.; Millange, F.; Morcrette, M.; Serre, C.; Doublet, M. L.; Grenèche, J. M.; Tarascon, J. M. *Angew. Chem., Int. Ed.* **2007**, *46*, 3259.

(27) Li, X. X.; Cheng, F. Y.; Zhang, S. N.; Chen, J. *J. Power Sources* **2006**, *160*, 542.

(28) Tran-Van, P.; Barthelet, K.; Morcrette, M.; Herlem, M.; Tarascon, J. M.; Cheetham, A. K.; Férey, G. *J. New Mater. Electrochem. Syst.* **2003**, *6*, 29.

(29) Cheng, C. Y.; Fu, S. J.; Yang, C. J.; Chen, W. H.; Lin, K. J.; Lee, G. H.; Wang, Y. *Angew. Chem.* **2003**, *115*, 1981; *Angew. Chem., Int. Ed.* **2003**, *42*, 1937.

(30) (a) Goodenough, J. B.; Kim, Y. *Chem. Mater.* **2010**, *22*, 587. (b) Kim, Y.; Arumugam, N.; Goodenough, J. B. *Chem. Mater.* **2008**, *20*, 470. (c) Combarieu, G.; Hamelet, S.; Millange, F.; Morcrette, M.; Tarascon, J. M.; Férey, G.; Walton, R. I. *Electrochem. Commun.* **2009**, *11*, 1881.

(31) (a) Satya Kishore, M.; Pralong, V.; Caignaert, V.; Varadaraju, U. V.; Raveau, B. *Solid State Sci.* **2008**, *10*, 1285. (b) Daidouh, A.; Veiga, M. L.; Pico, C. *Solid State Ionics* **1998**, *106*, 103.

(32) Sheldrick, G. M. *SHELXTL-97, Program for X-ray Crystal Structure Determination*; Göttingen University: Germany, 1997.

(33) (a) Zheng, X. J.; Li, L. C.; Gao, S.; Jin, L. P. *Polyhedron.* **2004**, *23*, 1257. (b) Ma, C.; Chen, C.; Liu, Q.; Liao, D.; Li, L.; Sun, L. *New J. Chem.* **2003**, *27*, 890.

(34) Liu, Q.; Li, B. L.; Xu, Z.; Sun, X. Q.; Yu, K. B. *Transition Met. Chem* **2002**, *27*, 786.

(35) Liu, Q.; Li, B. L.; Xu, Z.; Yu, K. B. *J. Coord. Chem.* **2003**, *56*, 771.

(36) (a) Liu, Q.; Li, Y. Z.; Song, Y.; Liu, H. J.; Xu, Z. *J. Solid State Chem.* **2004**, *177*, 4701. (b) Li, X. M.; Wang, C. F.; Ji, Y.; Kang, L. C.; Zhou, X. H.; Zuo, J. L.; You, X. Z. *Inorg. Chem.* **2009**, *48*, 9166.

(37) (a) Catalina, R. P.; Pablo, A. L.; María, H. M.; Milagros, L. M.; Pedro, G. *Crystal Growth Des.* **2004**, *4*, 57. (b) Li, M.; Xu, Z.; You, X.; Dong, Z.; Guo, G. *Polyhedron* **1993**, *12*, 921. (c) Li, M.; Xie, G. Y.; Gu, Y. D. *Polyhedron* **1995**, *14*, 1235.

(38) Mirhashemihaghighi, S.; León, B.; Vicente, C. P.; Tirado, J. L.; Stoyanova, R.; Yoncheva, M.; Zhecheva, E.; Puche, R. S.; Arroyo, E. M.; de Paz, J. R. *Inorg. Chem.* **2012**, *51*, 5554.

(39) Wagner, C. D.; Riggs, W. M.; Davis, L. E.; Moulder, J. F.; Muilenberg, G. E. *Handbook of X-Ray Photoelectron Spectroscopy*; Perkin-Elmer Corp.: Eden Prairie, MN, 1979.

(40) Saravanan, K.; Nagarathinam, M.; Balaya, P.; Vittal, J. J. *J. Mater. Chem.* **2010**, *20*, 8329.

(41) (a) Park, M. S.; Wang, G. X.; Kang, Y. M.; Wexler, D.; Dou, S. X.; Liu, H. K. *Angew. Chem., Int. Ed.* **2007**, *46*, 750. (b) Wang, G. X.; Wang, B.; Wang, X.; Park, J.; Dou, S. X.; Ahn, H.; Kim, K. *J. Mater. Chem.* **2009**, *19*, 8378.

(42) Hassoun, J.; Lee, K.-S.; Sun, Y.-K.; Scrosati, B. *J. Am. Chem. Soc.* **2011**, *133*, 3139.